An approach to morphing structure control based on real-time displacement reconstruction

Journal of Physics:
Conference Series

PAPER • **OPEN ACCESS**

An Approach to Morphing Structure Control based on Real-time Displacement Reconstruction

To cite this article: R Roy *et al* 2026 *J. Phys.: Conf. Ser.* **3253** 012004

Journal of Physics: Conference Series **3253** (2026) 012004 doi:10.1088/1742-6596/3253/1/012004

An Approach to Morphing Structure Control based on Real-time Displacement Reconstruction

R Roy[1], C Surace[2] and M Gherlone[1]

[1]Department of Mechanical & Aerospace Engineering, Politecnico di Torino, Italy
[2]Department of Structural, Geotechnical and Building Engineering, Politecnico di Torino, Italy

E-mail: `rinto47roy@gmail.com`

Abstract. Shape morphing structures are a key technology for the next generation of aerospace vehicles, facilitating adaptive performance based on their operational environment. This paper introduces a novel framework for morphing monitoring and control based on the inverse problem of reconstructing structural displacements using in-situ strain-sensor data, referred to as shape sensing. The inverse Finite Element Method (iFEM) is the inverse methodology employed, where the structure is discretised using a series of finite elements, and the displacements are reconstructed by minimizing a functional defined as the least-squares error between experimental and analytically defined strains. At each time step, the morphing actuation load is calculated by minimising the least-squares error between the desired and iFEM reconstructed nodal displacements. Real-time assessment of shape or displacement over the entire structural domain is expected to produce more accurate and efficient morphing performance. This novel control strategy is demonstrated numerically for the case of a morphing wing aircraft, where the shape of the wing section is controlled using a distributed set of actuators. The morphing performance in controlling the wing camber is investigated, and the effect of the number of actuators used is also studied. The preliminary numerical results demonstrate efficient control performance with the potential for further improvement.

1. Introduction

Structural morphing can be broadly defined as the functional change in the shape of a structure during operation. Nature provides abundant examples of such structures, e.g., insects and birds produce continuous variations in wing planform, camber, and twist during flight [1]. In contrast, human innovations in flight have led to the development of rigid aircraft designs that are often optimised for specific flight speeds or conditions and lack adaptability [2]. Development of morphing incorporated flight designs that improve efficiency and facilitate multi-mission adaptivity remains a key objective of research in the aerospace community [3]. For the case of an aircraft wing, this can be large-scale changes in planform area and sweep, or on a smaller scale with changes in the wing twist and cross-sectional profile (e.g., airfoil camber). Recent advances in this area have led to the development of morphing wings integrated with smart sensors and actuators (such as shape memory alloys (SMA) or piezoelectric), leading to more compact, efficient, and adaptable wing designs [3, 4]. Despite these advances, their future adoption is contingent on the development of certain key technologies [2, 5]: small and efficient actuators for shape or state change, and control algorithms to integrate sensors and actuators.

In existing literature, the most common morphing designs are those related to changes in wing profile or camber often involving kinematic rigid link mechanisms actuated by electromechanical actuators [6, 7, 8]. They have been demonstrated for the flap control of civil aircraft, featuring control schemes using encoders that measure relative rotation between links [6]. Alternatively, Fibre Bragg Grating (FBG) sensor measurements have also been used to develop control schemes to monitor wing bending and torsional deformations using a priori estimated transfer functions [7]. Similar leading-edge wing designs for variable cruise and take-off or landing performance have also been designed [8], and shape control using accelerometer measurements coupled with analytical, linear aeroelastic models has been proposed [9]. Other actuation alternatives include piezoelectric or SMA actuators, which necessitate more compliant wing designs due to the lower actuation force generated. Such designs include SMA actuators coupled with a fuzzy logic-based PID controller for controlling flow separation over an airfoil [10], and a distributed trailing edge morphing concept using piezoelectric actuators for load alleviation, and flutter suppression [11]. Recently, various control techniques based on reinforcement learning have also been proposed to develop the next generation of efficient morphing control systems [12]. Despite these advances, the development of morphing aircraft has largely remained theoretical, with very few designs finding industrial acceptance.

In this context, a topic of extreme relevance for morphing structure development, but one that has received very limited attention, is the problem of shape sensing. It is defined as the inverse problem of reconstructing the deformed shape of a structure using surface strain measurements. Various shape sensing methodologies have been proposed in literature [13] and have been identified to play a key role in the real-time condition and health monitoring of future aerospace vehicles. As the structural shape is reconstructed in real-time, shape sensing results can aid in developing real-time shape-based feedback control strategies for morphing structures. The development of such a coupled control strategy forms the basis of this work, and the inverse Finite Element Method (iFEM) [14, 15] is the specific shape sensing methodology used for this purpose. The iFEM is a variationally-based approach that solves for the displacement field by minimising an error functional defined as the least-squares error between analytical and experimentally measured strains. As it is based on the strain-displacement relations, it is inherently independent of the material properties and loading conditions of the structure and has been demonstrated to provide accurate and robust results even using a sparse set of strain data [14]. This work aims to employ the iFEM reconstructed displacements for developing open and closed-loop control strategies to monitor and control shape morphing structures under various simple and complex operational conditions.

The paper is organised as follows: Sections 2 and 3 introduce the open and closed-loop control schemes, discussing the underlying theory and the use of iFEM feedback. The open-loop control is demonstrated numerically in Section 4 for controlling the trailing edge shape of an airfoil wing section. Finally, Section 5 presents the main conclusions and avenues for future work.

2. Open-Loop Control

The structure monitored, whether it be a 1D beam or frame, or a 2D plate or shell, is assumed to be defined in the three-dimensional orthogonal Cartesian coordinate system $\mathbf{x} \equiv \{x, y, z\}$. The control formulation is based on discretising the structural geometry using a set of n nodes. At any time t, each node, i, is defined by its Cartesian coordinates, $\mathbf{P}_i(t) \equiv \{x, y, z\}_i^T$, and the global shape of the structure is given by the vector of nodal coordinates, $\mathbf{P}(t)_{[3n\times1]} = \{\mathbf{P}_i(t)\}$ (the subscript $[* \times *]$ indicates the vector/matrix dimensions). Change in shape of the structure over a time Δt is given by the change in the nodal coordinate vector as (see Fig. 1),

$$\mathbf{P}(t + \Delta t) = \mathbf{P}(t) + \mathbf{U}(t) \tag{1}$$

where, $\mathbf{U}(t)_{[3n\times1]} = \{\mathbf{U}_i(t)\}$ is the nodal displacement vector. The nodal coordinate change, $\mathbf{U}_i(t) = \{u, v, w\}_i^T$, is described in terms of the variables, u, v, and w, defined as the nodal displacements along the x, y, and $z-$axis, respectively.

Journal of Physics: Conference Series **3253** (2026) 012004 doi:10.1088/1742-6596/3253/1/012004

The proposed control strategy aims to accomplish a change of shape from an initial to a desired or reference shape. The reference shape is defined by the vector, $\mathbf{P}_{ref}$, and the corresponding nodal displacements required is defined by $\mathbf{U}_{ref}$. Assuming the reference shape to be a constant over a time Δt, the desired shape change can be described as,

$$\mathbf{P}(t+\Delta t) = \mathbf{P}(t) + \mathbf{U}_{ref}(t) \equiv \mathbf{P}_{ref} \tag{2}$$

The shape change is effectuated by a series of actuators instrumented on the structure (shown in Fig. 1). The forces and moments generated at any node, j, due to the actuators is represented by the vector, $\mathbf{L}_j(t) = \{N_x, N_y, N_z, M_x, M_y, M_z\}_j^T$, where N_x, N_y, N_z, are concentrated forces along the x, y, and $z-$axis, respectively, and M_x, M_y, M_z, are concentrated moments about the x, y, and $z-$axis, respectively. The total force is given by the vector, $\mathbf{L}(t)_{[6m\times 1]} = \{\mathbf{L}_j(t)\}$, where m represents the number of nodes where actuation loads are applied. At any time t, the instantaneous nodal displacements generated by these actuation loads is given as,

$$\mathbf{U}(t) = \mathbf{A}\mathbf{L}(t) \tag{3}$$

where $\mathbf{A}_{[3n\times 6m]}$ is referred to as the matrix of influence coefficients. Each column of $\mathbf{A}$ represents the nodal displacement vector due to a unit force or moment at a particular node of the structure, e.g., the first column represents $\mathbf{U}$ due to a unit N_x load at node 1. The present formulation aims to identify the load vector, $\mathbf{L}$, that generates the desired nodal displacements, $\mathbf{U}_{ref}$. This is accomplished by a functional defined as the weighted least-squares error between the actual and desired nodal displacements,

$$\Phi_m = ||\mathbf{U}_{ref} - \mathbf{U}(t)||^2 = \frac{1}{2}\mathbf{L}^T\mathbf{K}\mathbf{L} - \mathbf{L}^T\mathbf{F} + \mathbf{C} \tag{4}$$

where matrix $\mathbf{K}$ is only a function of the number and location of actuators used, while vector $\mathbf{F}$ is a function of the actuator position and reference shape of the structure. These quantities can be further defined as,

$$\mathbf{K} = \sum_{i=1}^{3n} \lambda_i \mathbf{A}_i^T \mathbf{A}_i \qquad \mathbf{F} = \sum_{i=1}^{3n} \lambda_i \mathbf{A}_i^T (\mathbf{U}_{ref})_i \tag{5}$$

where the subscript $(\bullet)_i$ represents the i^{th} row of a matrix or a vector, and $\boldsymbol{\lambda}$ is the weighting coefficient vector used to associate a value of weight, λ_i, to each nodal displacement component of $\mathbf{U}$. High ($\lambda_i = 1$) or low ($\lambda_i = 10^{-2} - 10^{-4}$) values are used to enforce a stronger or weaker correlation between the initial and desired nodal displacements. In cases where the morphing accuracy is poor, the values of weights can be used to exert a degree of control over the shape achieved, i.e., nodal displacements with higher weights will better approximate the desired value compared to those with lower weights. Hence, the morphed shape at certain key areas of the structure can be given more emphasis, e.g., the leading or trailing edge of an aircraft wing, to maximise structural performance.

The functional of Eq. 4 is minimised with respect to the nodal actuation loads to obtain a series of linear algebraic equations,

$$\mathbf{K}\mathbf{L} = \mathbf{F} \tag{6}$$

If $\mathbf{K}$ is ensured to be non-singular, Eq. 6 can be solved by matrix inversion to obtain the nodal actuation loads, $\mathbf{L}$, required to achieve the desired shape at the next time step. Prior knowledge of the influence matrix, $\mathbf{A}$, is key to implementing the present control strategy. This can be determined experimentally or numerically, and any inaccuracies in its estimation can lead to poor results. The control strategy in the present case is termed an open-loop because the final shape achieved is not evaluated to guarantee successful morphing. This capability is essential for more challenging morphing problems and hence is discussed in the next section.

Journal of Physics: Conference Series **3253** (2026) 012004 doi:10.1088/1742-6596/3253/1/012004

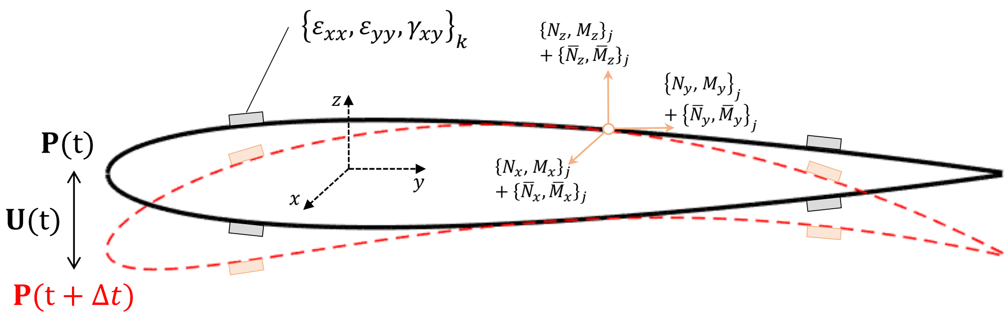

Figure 1: The initial and final shape acquired by a shape morphing airfoil over a time period Δt; the nodal actuation loads and the surface instrumented strain sensors are shown

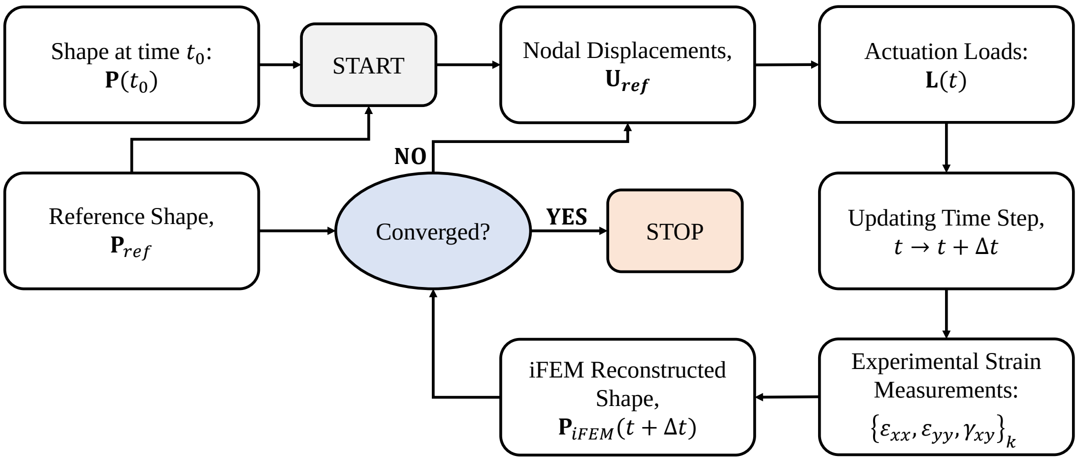

Figure 2: Flow diagram illustrating the main steps of the closed-loop control strategy

3. Closed-Loop Control

When a low number of actuators are used ($m << n$) or structural morphing is influenced by external loads, the open-loop strategy of Section 2 may be unsuccessful in achieving the desired shape, i.e., $\mathbf{P}(t+\Delta t) \neq \mathbf{P}_{ref}$. This is also true if the desired shape is a function of time, $\mathbf{P}_{ref}(t)$, or of the operational conditions of the structure. In such cases, the reference shape can only be achieved after multiple iterations. Hence a closed-loop control strategy based on feedback information regarding the shape of the structure is essential.

The iFEM forms the basis for the closed-loop control, providing real-time feedback regarding the structural shape using surface strain measurements. Both 1D iFEM for beam and frames and 2D iFEM for plates and shells have been developed and can be utilised depending on the structure analysed [13]. For the closed-loop control, the structure (a plate in this case) is also instrumented with strain sensors at N discrete locations, $\mathbf{x}_k \equiv \{x, y, z\}_k$, $(k = 1, ..., N)$, measuring strains, $\{\varepsilon_{xx}, \varepsilon_{yy}, \gamma_{xy}\}_k^{\pm}$ on the top and bottom surface of the plate. The strain measurements at any time t are used to compute the iFEM reconstructed shape, $\mathbf{P}_{iFEM}(t)$, which is subsequently used as feedback for the next time step.

Assuming the structure while morphing to be influenced by external loads (e.g., the

Journal of Physics: Conference Series **3253** (2026) 012004 doi:10.1088/1742-6596/3253/1/012004

aerodynamic loads on aircraft wing), the total load at any node j of the structure is the superposition of actuation loads, $\mathbf{L}_j(t)$, and nodal contributions due to the unknown external load, $\mathbf{M}_j(t) = \{\overline{N}_x, \overline{N}_y, \overline{N}_z, \overline{M}_x, \overline{M}_y, \overline{M}_z\}_j^T$. The corresponding overall load vectors are, $\mathbf{L}(t)_{[6m\times 1]} = \{\mathbf{L}_j(t)\}$, and $\mathbf{M}(t)_{[6m\times 1]} = \{\mathbf{M}_j(t)\}$. For an actuation load, $\mathbf{L}(t)$, the resultant nodal displacement can now be written as,

$$\mathbf{U}(t) = \mathbf{A}\left(\mathbf{L}(t) + \mathbf{M}(t)\right) \tag{7}$$

Substituting Eq. 7 in Eq. 1 demonstrates that the desired shape is not achieved at $t + \Delta t$,

$$\mathbf{P}(t+\Delta t) = \mathbf{P}(t) + \mathbf{A}\left(\mathbf{L}(t) + \mathbf{M}(t)\right) \neq \mathbf{P}_{ref} \tag{8}$$

Due to the inaccuracies of the shape achieved, iFEM-based shape feedback, $\mathbf{P}_{iFEM}$, is used to update the actuation load applied. For an accurate iFEM reconstruction,

$$\mathbf{P}_{iFEM}(t+\Delta t) \equiv \mathbf{P}(t+\Delta t) \tag{9}$$

Using the iFEM contribution, the desired nodal displacement vector is updated as,

$$\mathbf{U}_{ref}(t+\Delta t) = \mathbf{P}_{ref}(t+\Delta t) - \mathbf{P}_{iFEM}(t+\Delta t) \tag{10}$$

Substituting Eq. 10 in Eq. 4, the updated actuation load, $\mathbf{L}(t+\Delta t)$, corresponding to $\mathbf{U}_{ref}(t+\Delta t)$ is computed. In the present case, as the shape inaccuracy is due to the external load, Eq. 10 implies the change in actuation load to be,

$$\Delta\mathbf{L}(t+\Delta t) = \mathbf{L}(t+\Delta t) - \mathbf{L}(t) \approx \mathbf{M}(t) \tag{11}$$

However, as $\mathbf{M}(t)$ is unknown, it cannot be used directly in the control strategy, and the updated load, $\mathbf{L}(t+\Delta t)$ is estimated inversely using Eq. 4. The success of the closed-loop strategy is contingent on the ability of iFEM to accurately reconstruct the structural shape (stated in Eq. 9). iFEM inaccuracies can lead to $\mathbf{P}(t+2\Delta t) \neq \mathbf{P}_{ref}$, and requiring further time steps to converge to an accurate shape.

As mentioned previously, prior and accurate estimation of the influence matrix, $\mathbf{A}$, is key to the present control strategy. When direct experimental or numerical estimation is difficult or impossible, the iFEM reconstructed nodal displacements corresponding to individual actuation loads can be used to compute an iFEM-based influence matrix, $\mathbf{A}_{iFEM} \equiv \mathbf{A}$. Such an approach leads to significant practical ease and the possibility of a finer discretisation of the morphing structure. Here again, the iFEM accuracy is a key factor influencing the final morphing results obtained. A detailed description of the iFEM is not within the scope of the present paper. Interested readers are encouraged to refer to Ref. [14, 15] for more details. The flowchart of this closed-loop control strategy is shown in Fig. 2.

4. Numerical Results

The novel control strategy introduced in this work is evaluated numerically for the problem of controlling the trailing edge shape of an aircraft wing. The structure analysed is shown in Fig. 3a, and represents only a small section of a hypothetical future morphing aircraft wing. It has a NACA 6516 airfoil profile of chord length 1 m and is composed of multiple stiffening spar and rib elements of thickness 5 mm. The material for the wing design is a glass fibre reinforced composite. The trailing edge of this wing section (highlighted in red in Fig. 3a) is deformed by a set of distributed actuators (sixteen in total) placed on the upper and lower surface, as shown in Fig. 4, and generating concentrated moments along the trailing edge.

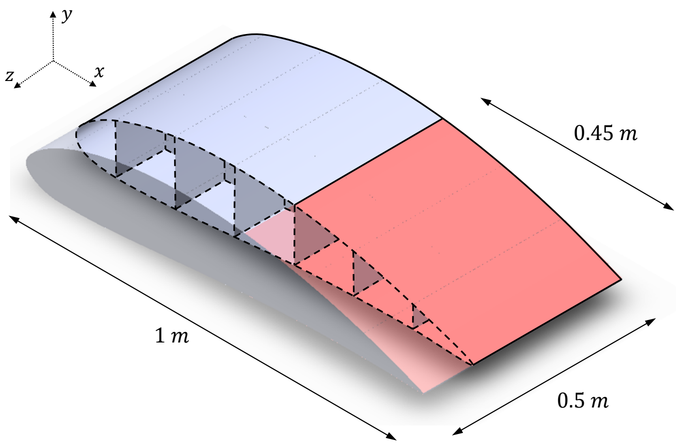

(a)

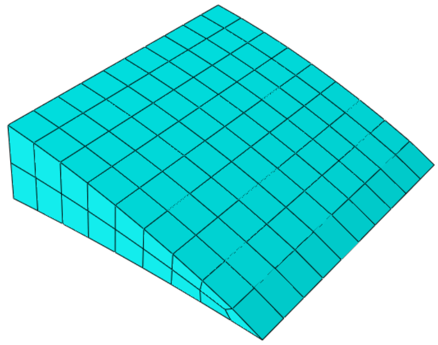

(b)

Figure 3: Airfoil section analysed: (a) rendering of the morphing airfoil structure (sectional view is used to show the internal stiffening elements), and (b) FEM mesh of the trailing edge

The present preliminary investigation aims to assess the capability of the open-loop control strategy to compute the actuation moments required to execute a predefined shape change. For this purpose, only the trailing edge of the section is analysed. As it is connected to a central spar of the wing (which is much stiffer), the internal boundary of the trailing edge is assumed to be fixed. To simulate structural behaviour under an actuation load, a numerical model of the trailing edge is developed in ABAQUS using 291 four-node shell elements (S4R). The FEM mesh also serves as the nodal discretisation for the control strategy. The FEM model is used to define the reference displacement of the trailing edge and simulate the shape achieved based on the actuation loads prescribed by the control strategy.

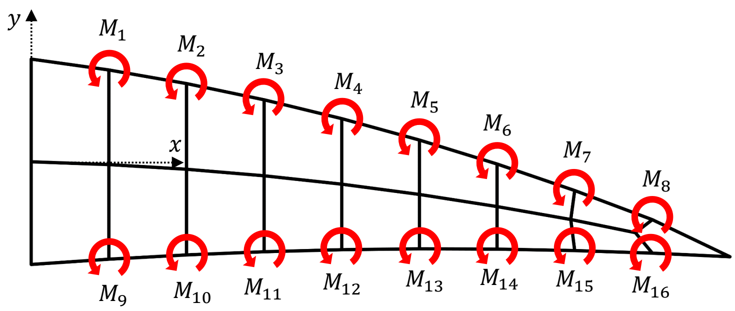

Figure 4: The distributed actuator positions along the airfoil trailing edge

Two different approaches are used to determine the influence coefficient matrix: the first using FEM ($\mathbf{A}_{\mathrm{FEM}}$), and the second using iFEM reconstructed nodal displacements ($\mathbf{A}_{\mathrm{iFEM}}$). For the iFEM analysis, 291 four-node quadrilateral elements (iQS4) are used to model the wing section. For the present problem, all inverse elements on the top and bottom skin of the structure are instrumented with strain sensors. The numerical strains required for the iFEM procedure are extracted from this FEM model, and the FEM reconstructed displacements are used as a reference for iFEM comparisons. The reference displacement field for the present analysis is defined by the reference actuator loads of Table 1.

Table 1: The reference and estimated actuator loads (all moments are in Nm)

Case	M_1	M_2	M_3	M_4	M_5	M_6	M_7	M_8
Reference	-40	-35	-30	-25	-20	-15	-10	-5
Set-1 | $\mathbf{A}_{\text{FEM}}$	-40	-35	-30	-25	-20	-15	-10	-5
Set-1 | $\mathbf{A}_{\text{iFEM}}$	-80.0	-71.3	-74.6	-58.4	-52.4	-40.2	-33.8	-22.8
Set-2 | $\mathbf{A}_{\text{FEM}}$	-51.3	-37.4	0	-31.5	-25.4	0	-32.2	-23.1
Set-2 | $\mathbf{A}_{\text{iFEM}}$	-48.9	-49.4	0	-33.4	-21.3	0	-36.9	-22.4
Case	M_9	M_{10}	M_{11}	M_{12}	M_{13}	M_{14}	M_{15}	M_{16}
Reference	-40	-35	-30	-25	-20	-15	-10	-5
Set-1 | $\mathbf{A}_{\text{FEM}}$	-40	-35	-30	-25	-20	-15	-10	-5
Set-1 | $\mathbf{A}_{\text{iFEM}}$	-0.6	-3.3	8.5	5.2	11.5	9	11.6	11.8
Set-2 | $\mathbf{A}_{\text{FEM}}$	-53.2	-43.2	0	-37.5	-41.5	0	8.6	5.9
Set-2 | $\mathbf{A}_{\text{iFEM}}$	-43.1	-51.5	0	-40.5	-42.2	0	10.8	6.3

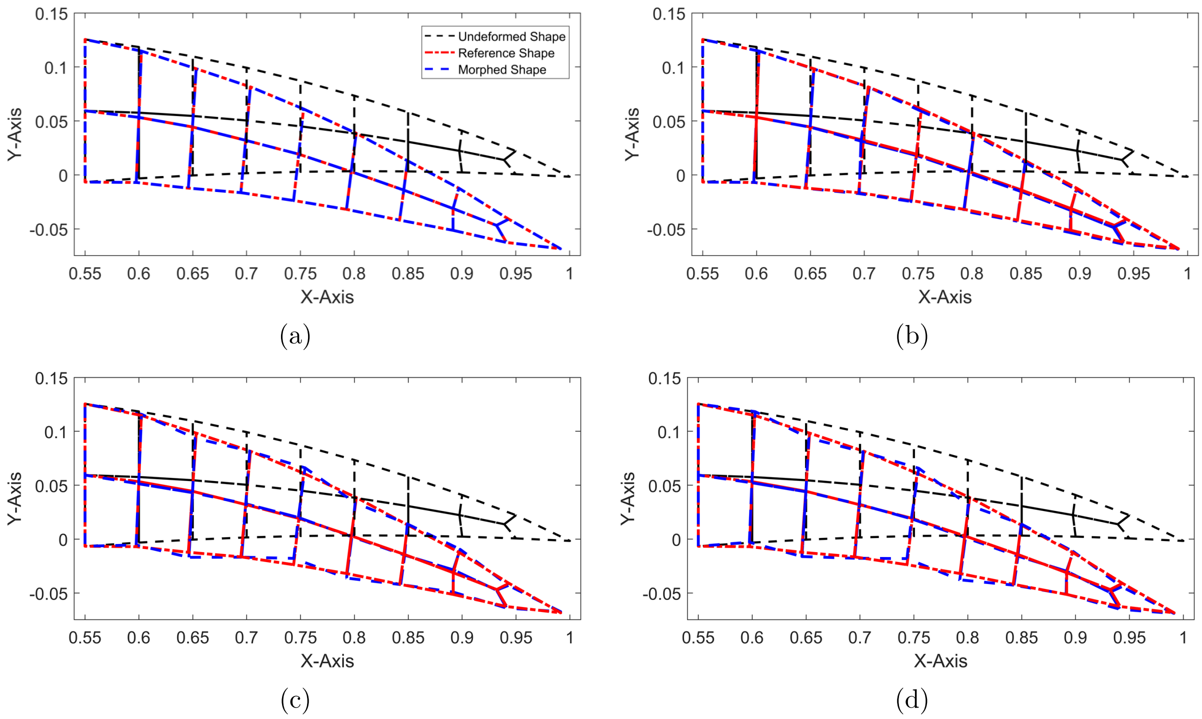

Figure 5: Morphed shape of the central rib of the structure based on the actuation loads of Table 1 (axes dimensions are in m and the deformation scale factor = 10^3): (a) Set-1 | $\mathbf{A}_{\text{FEM}}$, (b) Set-1 | $\mathbf{A}_{\text{iFEM}}$, (c) Set-2 | $\mathbf{A}_{\text{FEM}}$, and (d) Set-2 | $\mathbf{A}_{\text{iFEM}}$

Two different actuator configurations are used to control the shape: Set-1, where all sixteen actuators are used, and Set-2, which is a more discrete case with M_3, M_6, M_{11}, and M_{14} left unused. The actuator loads computed by the control strategy are reported in Table 1, while the corresponding deformed shape of the central rib is plotted in Fig. 5. For Set-1, the difference in actuator loads calculated based on the two influence matrices is attributed to the inaccuracies in the iFEM reconstruction. Despite these differences, the final morphed shape is equally accurate. For Set-2, the computed actuator loads are again different, but they result in a reasonably accurate morphed shape with minor local shape inaccuracies. These minor accuracies are attributed to the absence of the full set of actuators. These results highlight the capability of the proposed control strategy to achieve the required shape for different approaches ($\mathbf{A}_{\mathrm{FEM}}$ and $\mathbf{A}_{\mathrm{iFEM}}$) and using a full (Set-1) and reduced set of actuators (Set-2).

5. Conclusions

A novel control strategy is proposed based on the inverse Finite Element Method for open and closed-loop control of shape morphing structures. The strategy involves discretising the structural domain into a set of nodes. The actuation force required to achieve the shape change is computed by minimising a functional described as the least-squares error between the reference and iFEM reconstructed nodal displacements. Open-loop control performance was demonstrated numerically for controlling the airfoil trailing edge shape of a wing section and revealed the preliminary morphing results to be accurate. Future work will investigate the closed-loop control for structures influenced by external loads.

References

[1] Valasek, J.: Morphing Aerospace Vehicles and Structures. John Wiley & Sons Inc, Chichester, UK (2012)

[2] Weisshaar, T. A.: Morphing aircraft systems: Historical perspectives and future challenges. Journal of Aircraft **50**(2), 337-353 2013

[3] McGowan, A.-M. R.; Washburn, A. E.; Horta, L. G.; Bryant, R. G.; Cox, D. E.; Siochi, E. J.; Padula, S. L.; Holloway, N. M.: Recent Results from NASA's Morphing Project [C]. SPIE's 9th Annual International Symposium on Smart Structures and Materials **4698**, 97-111 2002

[4] Barbarino, S.; Bilgen, O.; Ajaj, R. M.; Friswell, M. I.; Inman, D. J.: A review of morphing aircraft. Journal of Intelligent Material Systems and Structures **22**(9), 823-877 (2011)

[5] Sofla, A. Y. N.; Meguid, S. A.; Tan, K. T.; Yeo, W. K.: Shape morphing of aircraft wing: Status and challenges. Materials and Design **31**(3), 1284-1292 2010

[6] Pecora, R.: Morphing wing flaps for large civil aircraft: Evolution of a smart technology across the Clean Sky program. Chinese Journal of Aeronautics **34**(7), 13-28 2021

[7] Nazeer, N.; Wang, X.; Groves, R. M.: Sensing, actuation, and control of the smartx prototype morphing wing in the wind tunnel. Actuators **10**(6), 1-20 2021

[8] Asins, C. C.; Landersheim, V.; Laveuve, D.; Adachi, S.; May, M.; Wacker, J. D.; Decker, J.: Analysis and design of a leading edge with morphing capabilities for the wing of a regional aircraft—gapless chord-and camber-increase for high-lift performance. Applied Sciences (Switzerland) **11**(6), 6 2011

[9] Whitmer, C. E.; Kelkar, A. G.: Robust control of a morphing airfoil structure. Proceedings of the American Control Conference **4**, 2863-2868 2005

[10] Grigorie, T. L.; Botez, R. M.; Popov, A. V.; Mamou, M.; Mébarki, Y.: A hybrid fuzzy logic proportionalintegral-derivative and conventional on-off controller for morphing wing actuation using shape memory alloy Part 2: Controller implementation and validation. Aeronautical Journal **116**, 451-465 2012

[11] Mkhoyan, T.; Thakrar, N. R.; Breuker, R. D.; Sodja, J.: Design and development of a seamless smart morphing wing using distributed trailing edge camber morphing for active control. AIAA Scitech 2021 Forum, 1-16 2021

[12] Valasek, J.; Tandale, M. D.; Rong, J.: A reinforcement learning - Adaptive control architecture for morphing. Journal of Aerospace Computing, Information, and Communication **2**, 2005

[13] Gherlone, M.; Cerracchio, P.; Mattone, M.: Shape sensing methods: Review and experimental comparison on a wing-shaped plate. Progress in Aerospace Sciences **99**, 14-26 2018

[14] Tessler, A.; Spangler, J. L.: A least-squares variational method for full-field reconstruction of elastic deformations in shear-deformable plates and shells. Computer Methods in Applied Mechanics and Engineering **194**, 327-339 2005

[15] Roy, R.; Gherlone, M; Surace, C.: A shape sensing methodology for beams with generic cross-sections: Application to airfoil beams. Aer. Sci. and Tech. **110**, 106484 2021